

# Design and control of a proof-of-concept active jet engine intake using shape memory alloy actuators

Gangbing Song<sup>\*1</sup>, Ning Ma<sup>1</sup>, Luyu Li<sup>1</sup>, Nick Penney<sup>2</sup>, Todd Barr<sup>3</sup>,  
Ho-Jun Lee<sup>4</sup> and Steve Arnold<sup>5</sup>

<sup>1</sup>*Department of Mechanical Engineering, University of Houston, N207 Engineering Building 1,  
Houston, TX 77204-4006, USA*

<sup>2</sup>*Ohio Aerospace Institute (OAI), 22800 Cedar Point Road, Cleveland, OH 44142, USA*

<sup>3</sup>*Jackson & Tull Aerospace Division, Cleveland, OH 44135, USA*

<sup>4</sup>*NASA Johnson Space Center, Houston, TX, USA*

<sup>5</sup>*NASA Glenn Research Center, 21000 Brookpark Road, Cleveland, OH 44135, USA*

*(Received April 9, 2007, Accepted March 19, 2010)*

**Abstract.** It has been shown in the literature that active adjustment of the intake area of a jet engine has potential to improve its fuel efficiency. This paper presents the design and control of a novel proof-of-concept active jet engine intake using Nickel-Titanium (Ni-Ti or Nitinol) shape memory alloy (SMA) wire actuators. The Nitinol SMA material is used in this research due to its advantages of high power-to-weight ratio and electrical resistive actuation. The Nitinol SMA material can be fabricated into a variety of shapes, such as strips, foils, rods and wires. In this paper, SMA wires are used due to its ability to generate a large strain: up to 6% for repeated operations. The proposed proof-of-concept engine intake employs overlapping leaves in a concentric configuration. Each leaf is mounted on a supporting bar than can rotate. The supporting bars are actuated by an SMA wire actuator in a ring configuration. Electrical resistive heating is used to actuate the SMA wire actuator and rotate the supporting bars. To enable feedback control, a laser range sensor is used to detect the movement of a leaf and therefore the radius of the intake area. Due to the hysteresis, an inherent nonlinear phenomenon associated with SMAs, a nonlinear robust controller is used to control the SMA actuators. The control design uses the sliding-mode approach and can compensate the nonlinearities associated with the SMA actuator. A proof-of-concept model is fabricated and its feedback control experiments show that the intake area can be precisely controlled using the SMA wire actuator and has the ability to reduce the area up to 25%. The experiments demonstrate the feasibility of engine intake area control using an SMA wire actuator under the proposed design.

**Keywords:** shape memory alloy wire; Nitinol; jet engine intake; sliding mode control.

---

## 1. Introduction

Modern aircrafts use the jet engines to provide thrust. Intake is an important part of a jet engine and plays an important role in engine performance. Intakes with different shapes and sizes have been designed to achieve optimal performance under variant operating conditions. In literature, researchers have shown that the active adjustment of the intake area of a jet engine has potential to

---

<sup>\*</sup>Corresponding Author, Professor, E-mail: [gsong@uh.edu](mailto:gsong@uh.edu)

improve its fuel efficiency (Pitt *et al.* 2001). Shape Memory Alloy (SMA) material is a competitive candidate to provide actuation for a variable area intake due to its high power-weight ratio, solid-state actuation, and high corrosion resistance.

SMA refers to the alloy that has ability to return to a predetermined shape upon heating. This phenomenon is called shape memory effect (SME). As an SMA is cold, it is weak and undergoes a pseudo-plastic deformation under loading quite easily, i.e., it can be deformed to a new shape which remains after unloading. However, the new shape is not stable when the material's temperature is over the transformation temperature. A crystal transformation takes place at this temperature and the SMA transforms to the original shape. During this procedure, SMA can provide extremely large restoration force or large strain recovery. For example, the commonly used Nitinol, an alloy of nickel and titanium, is capable of up to 5% strain recovery for repeatable operations and 500 MPa restoration stress.

For SMA applications in the aeronautic engineering, the main benefit lies in the fact of its high power-to-weight ratio, as compared to the conventional actuators like electrical motors or hydraulic actuators. Rey *et al.* (2001) designed and fabricated an SMA bundled cable actuator to control a variable area fan nozzle. A feedback controller for this SMA actuated variable area fan nozzle was implemented by Barooah and Rey (2002). Epps and Chopra (2001) used an SMA wire actuator to correct the blade dissimilarities of a helicopter in flight. Wolf and Gunter (2001) investigated changing the geometry of the airfoil of a fixed wing using SMA actuators. Pitt *et al.* (2001) demonstrated a smart inlet funded by DARPA (Defense Advanced Research Project Agency) for supersonic flight. Strelec *et al.* (2003) utilized Genetic Algorithm (GA) to maximize the lift-to-drag ratio for a reconfigured airfoil shape with SMA wire actuators at subsonic flow conditions. Calkins *et al.* (2006) used shape memory alloy actuators to morph the shape of chevrons on the trailing edge of a jet engine to optimize acoustic and performance objectives at multiple flight conditions. Dayananda *et al.* (2007) proposed the SMA based smart landing gear design and development that is applicable to a radio controlled airship. Barbarino *et al.* (2009) presented a morphing wing trailing edge concept using SMA actuators. Peng *et al.* (2009) developed a simple control strategy based on the idea of adjusting the SMA wire temperature as rapidly as possible, which is used for active shape control of a membrane structure model by adjusting its boundary tensions.

This paper presents the design, testing and control of a novel proof-of-concept active jet engine intake using Nitinol shape memory alloy wire actuators. The rest of this paper is organized as follows. First, the design of the intake model is introduced. To examine the dynamic performance of the intake model under actuation by the SMA wire, preliminary open-loop tests are conducted. Based on the author's previous work, a nonlinear sliding-mode based robust controller is designed. Finally, the feedback control system is tested for both position regulation and tracking tasks.

## 2. Design of the proof-of-concept intake model

In order to demonstrate the feasibility of controlling the variable area intake using the Nitinol SMA actuator, a proof-of-concept intake model was designed and fabricated. Fig. 1 shows the front view of this model. This model mainly consists of four parts: eight overlapping leaves, eight supporting bars, the cylindrical frame structure, and the SMA wire actuator.

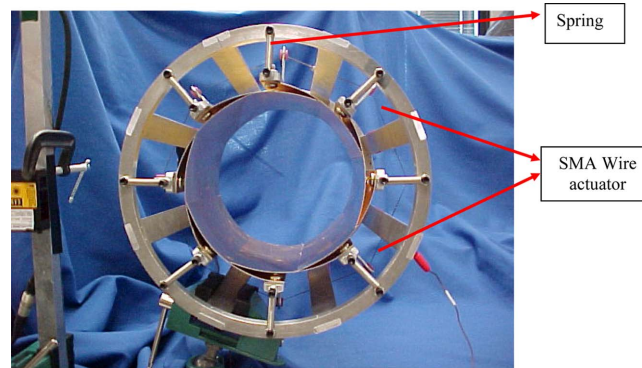


Fig. 1 The proof-of-concept jet engine intake model

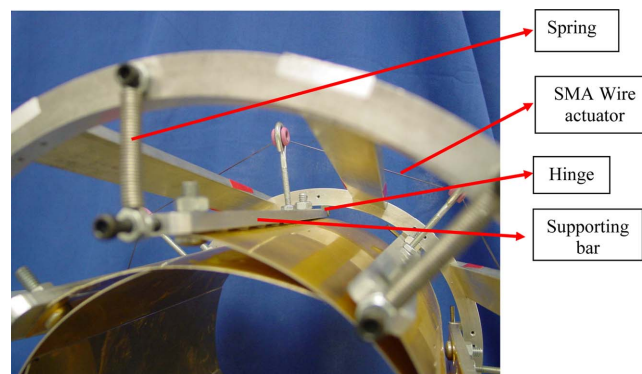


Fig. 2 A close-up view of the supporting bar

The inner wall of the model intake is constructed by overlapping the eight brass leaves in a concentric configuration. Each of the leaves is mounted on a supporting bar. The eight supporting bars are evenly distributed along the circumference of the cylindrical frame structure. One end of the supporting bar is hinged to the frame and the other end is constrained by a pre-strained extension spring. The SMA actuator, a group of three Nitinol wires of 0.015 inches in diameter, restrains the supporting bars in a ring format. The Austenite Finish (AF) temperature of the SMA wire is 90 degree C. Fig. 2 shows the close-up view of the supporting bar and the associated leave. When the SMA wire group shrinks upon electrical resistive heating, the supporting bars along with the leaves are pushed to move towards the center of the cylindrical frame. The intake area decreases accordingly. This action will further strain the extension springs. As the electrical current is removed, the SMA actuator is cooled and the strained extension springs pulls the supporting bars along with the overlapping leaves back to their original positions and the original area resumes.

The supporting bars also function as motion amplification mechanisms. This is to overcome the limited motion that than can be provided by the SMA actuator. The SMA wire actuator used here can only recovered 5% strain for repeatable operations. Consider the specific geometry of this intake model (Figs. 3 and 4), the SMA wire's deformation  $\Delta x$  can be expressed as a function of the tip displacement  $y$  of each supporting bar or the intake area change  $\Delta A$  as

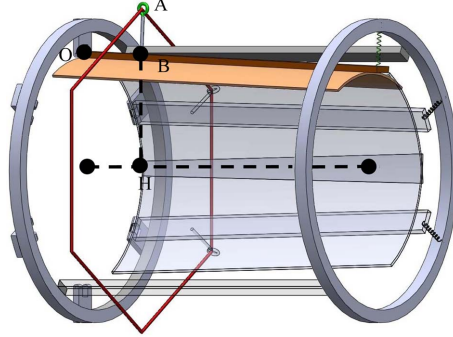


Fig. 3 Schematic diagram of the intake model

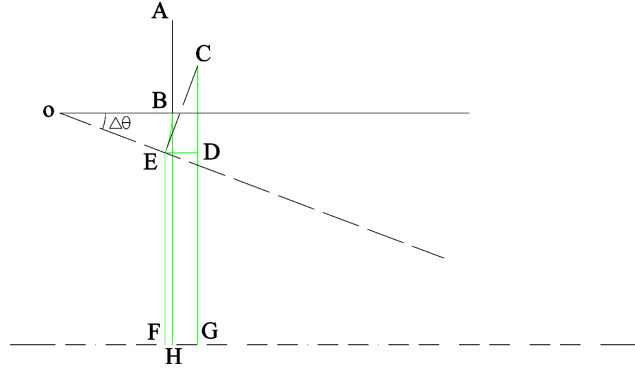


Fig. 4 Geometry analysis of the intake model

$$\Delta x = 2\pi \left[ L_2 + L_1 \frac{\Delta A}{2\pi r L} - L_2 \sqrt{1 - \left( \frac{\Delta A}{2\pi r L} \right)^2} \right] \quad (1)$$

or

$$\Delta x = 2\pi \left[ L_2 + L_1 \frac{y}{L} - L_2 \sqrt{1 - \left( \frac{y}{L} \right)^2} \right] \quad (2)$$

The detailed derivation with the help of Figs. 3 and 4 is show in the Appendix.

Eqs. (1) and (2) can be approximated by

$$\Delta x = 2\pi \frac{L_1}{2\pi r L} \Delta A = \frac{L_1}{r L} \Delta A \quad (3)$$

$$\Delta x = \frac{2\pi L_1}{L} y \quad (4)$$

where  $L$  is the bar length,  $L_1$  is the distance from the hinge to the point where contracting force from the SMA actuator is applied and  $L_2$  is the length of supporting bar. The detailed derivation is also shown in the Appendix (where  $y = \Delta r$ ,  $L_1 = OB$  and  $L_2 = AB$ ).

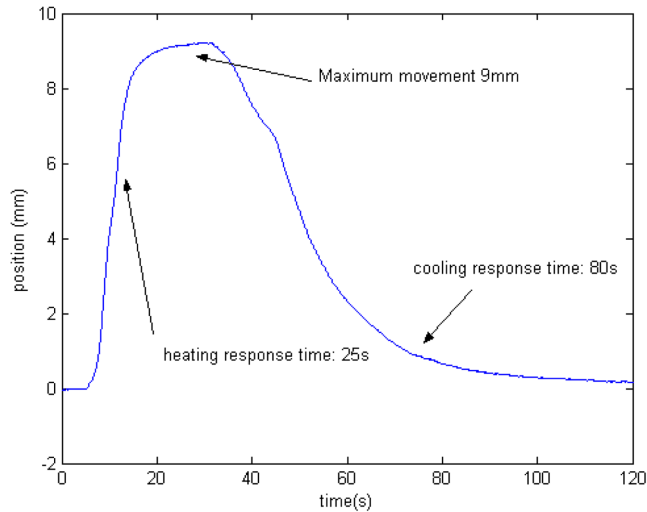


Fig. 5 The position response to a single-square wave input

### 3. Open-loop testing of the intake model

An experimental setup was developed to conduct open-loop testing and implement the feedback control of the intake prototype. The experimental setup consists of a digital data acquisition and real-time control system, a laser range sensor, a programmable power amplifier, and the intake model. The laser range sensor is employed to detect the tip displacement of one of the supporting bar. The area of the intake can be then easily computed. A programmable power amplifier drives the SMA wire group via electrical resistive heating.

In the open-loop testing of the intake, two kinds of input signals are applied to the SMA actuator: a single-square wave signal and a sinusoidal signal. The tests were conducted at the temperature of 22 degree C. From the response to a single-square wave (30 seconds heating) signal (Fig. 5), it is observed that the maximum tip displacement of the tip of the supporting bar is 9 mm, corresponding to a 25% area reduction of the intake. It is about 25 seconds for the SMA actuator to reach the maximum stroke, however, it takes a relatively longer time period (60-80 seconds) to resume the original area due to the slow heat dissipation. Please note that the heat dissipation here mainly depends on free convection. Therefore, for the square wave response, we can estimate that the minimum operating period is about 90 seconds for the SMA wire actuator at the temperature of 22 degree C. To improve the response of the device during cooling period in a laboratory setup, forced convection can be used.

Considering the estimated minimum operating period of about 90 seconds with an environment temperature of 22 degree C, tests of the SMA wire actuator with sinusoidal signals of 1/90 Hz and 1/120 Hz were conducted. Fig. 6 shows the tip responses of the supporting bar under actuation from these two different sinusoidal signals. The tip position reaches close to its extreme position of 9 mm in both cases of 1/90 Hz and 1/120 Hz. However, due to the slow response as in the cooling state, the SMA actuator does not have enough time to be cooled to go back to its initial position for the case of 1/90 Hz.

Fig. 7 shows the relationship between the input voltage signal and tip position of the supporting

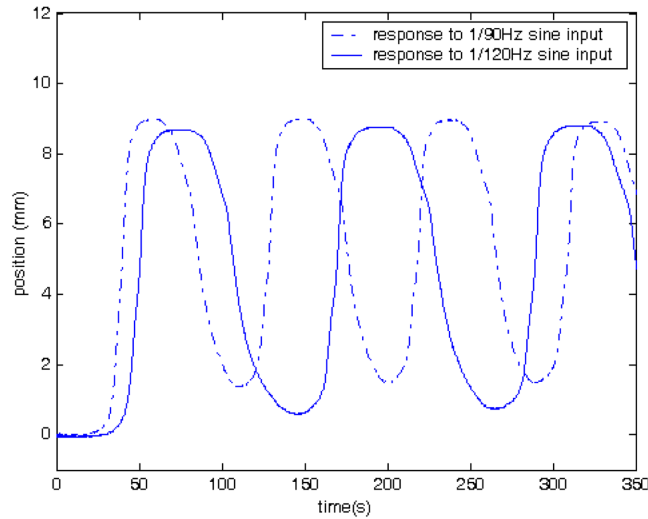


Fig. 6 The position responses to the sinusoidal inputs

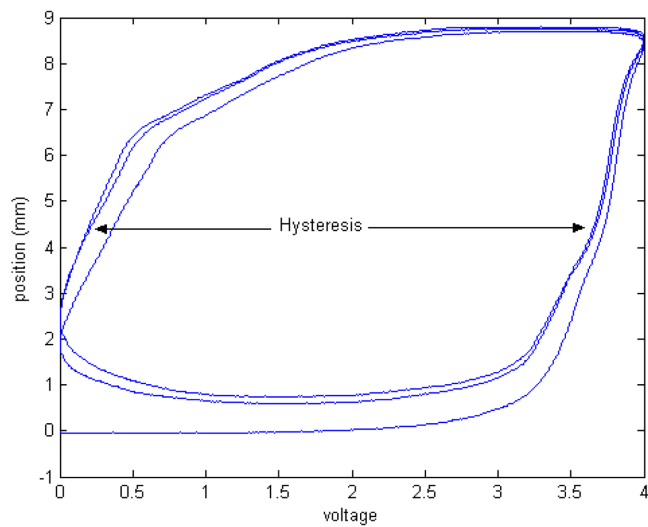


Fig. 7 The hysteretic relationship between the input voltage and the position

bar for the SMA wire actuator. It is clear that this relationship is hysteretic and this calls for advanced controls to achieve precise positioning.

Please note that the minimum operating period (operating bandwidth) will be dramatically shorter (increased), or the operating bandwidth will be greatly increased, for a real application where the engine intake is exposed to an extremely cold environment (-50 degree C or colder) at high elevation. However, it will also require more electric current to heat the SMA wire to its transformation temperature for actuation. By considering the required operating bandwidth and minimization of energy cost, an appropriate thermal insulation can be applied to the SMA wire actuator.

#### 4. Feedback control design

As mentioned in an early section, the opening area of the intake is desired to alter according to different flight conditions. A feedback control system will help to accomplish this task in a stable manner.

Since the object of the research is to control position of the supporting bar and therefore the opening area of the intake, only position sensor is used to simplify the control implementation. Though a temperature sensor is often used in control of an SMA actuator, in this paper, the feedback control is designed without the need of temperature information, which eliminates the need of temperature sensors.

One obstacle to the control system design is the hysteretic behavior of the SMA actuator. To achieve high precision and robust stability, nonlinear controls have to be used. Shown in Fig. 7 is the relationship between the input voltage signal and tip position of the supporting bar. It is clear that the relationship is highly hysteretic. The inherent hysteresis associated with SMA actuation is caused by the friction effect of the adjunct crystal layers during phase transformation. The SMA's hysteresis results in inaccurate positioning and possible instability with traditional linear controls.

In literature, a few control algorithms have been investigated for control of SMA actuators, for example, the proportional-integral (PI) control (Majima *et al.* 2001), the H-infinity controller (Choi *et al.* 2001) and the variable structure control (Grant and Hayward 1997).

In this paper, a nonlinear sliding-mode based smooth robust controller is used. This type of robust controller has been successfully applied to control of nonlinear systems with uncertainty, such as the robotic manipulators with joint friction and the SMA wire actuator (Song and Quinn 2000). The details of theoretic analysis for this type robust controller can be found in (Song and Mukherjee 1998).

Sliding mode control is a robust method to control high-order nonlinear systems with uncertainties. This method consists of two steps; the first step is to design a stable sliding mode surface to which the controller system trajectories will arrive. Then, a robust compensator will be designed to force the states to reach the sliding mode surface such that a sliding mode occurs on this manifold. When sliding mode is realized, the system exhibits robustness with respect to parameter variations and external disturbances.

There are three categories of the sliding-mode based robust compensators: the bang-bang controller, the saturation controller and the smooth time-varying controller employing a hyperbolic tangent function with time-varying gain (Song and Mukherjee 1998). The advantage of the smooth time-varying controller is that it not only eliminates the chattering that is a drawback of the bang-bang controller, but also guarantees the asymptotical stability. Consider the physical limitation of the position sensor, bounded stability satisfies the requirement for practical applications. In this paper, the smooth controller with a fixed gain will be used.

The SMA actuator will be controlled by applying a voltage on the SMA wire to achieve resistive heating. Let designate the applied voltage as  $u$ . The controller is proposed as

$$u = u_f - Kr - \rho \text{Tanh}(ar) \quad (5)$$

where  $u_f$  is a feedforward voltage and  $K$  is a positive constant. The  $\rho$  is an estimated upper bound of the all uncertainties associate with the intake actuated by the SMA actuator. The sliding surface variable is defined as  $r = \dot{e} + \lambda e$ , and  $e$  is the position control error.  $\lambda$  is a positive number. It is clear from (5) that the control action is composed of three parts: a feedforward action  $u_f$ , a Proportional plus

Derivative (PD) action  $Kr$  and the robust compensator  $-\rho \tanh(ar)$ .

The  $u_f$  is a feedforward action and it is defined as

$$u_f = k_f(T\dot{y}^d + y^d) \quad (6)$$

where  $k_f$  is a positive constant gain,  $T$  is a positive time constant, and  $y^d$  is the desired position command. The position refers to that of the tip of the supporting bar. This feedforward voltage is designed to provide the approximate amount of current required for the SMA actuator to follow the desired path. The actuator system with a bias spring is approximately a first order system with a time constant  $T$  if the current is considered as the input and the displacement is considered as the output. However, this first order model does not include the hysteretic nonlinearity. The effect of the mass of the moving parts and viscous friction in this system are neglected. In the experiment,  $T$  can be estimated based on the actuator's step responses.

The PD control action helps to increase the damping and to stabilize the system. The robust compensator is used to compensate for the hysteresis, other modeling uncertainties and external disturbances.

## 5. Experimental results

Experiments of real-time feedback control of the area adjustable intake model were conducted using the proposed sliding-mode based robust controller. Two types of tasks are used to evaluate the control performance. One is for the position regulation and the other is for tracking a sinusoidal command.

For position regulation tasks, first, the supporting bar is required to move 5 mm for 50 seconds before moving back to its original position. The position response in this case is shown in Fig. 8. In another test, the supporting bar is required to move 5 mm for 50 seconds then hold at the 2 mm

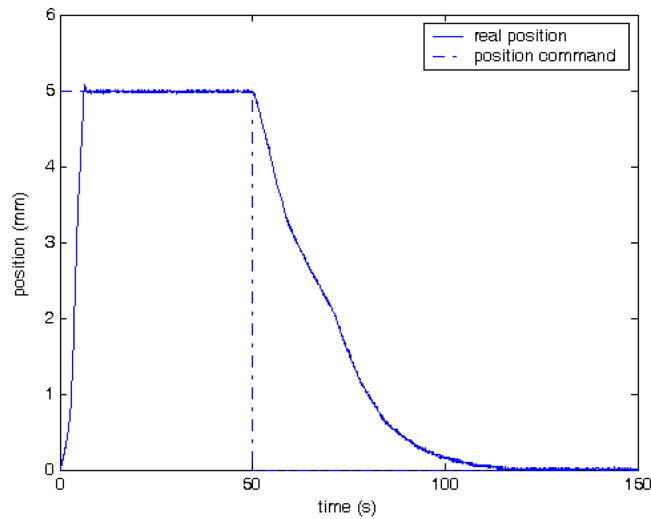


Fig. 8 The controlled position response to a position command

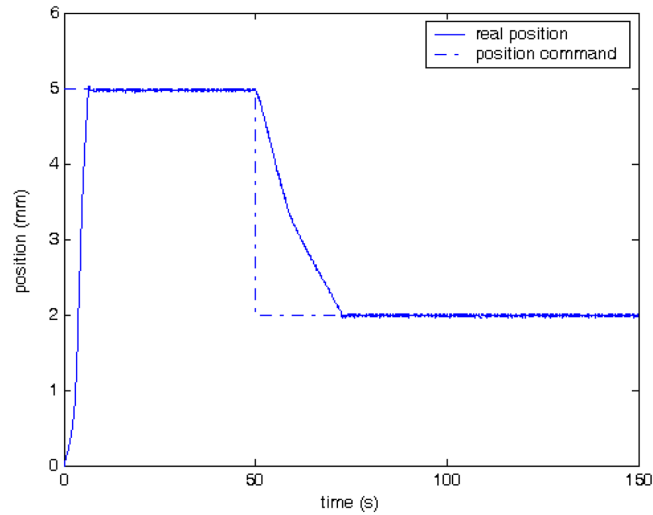


Fig. 9 The controlled position response to two position commands

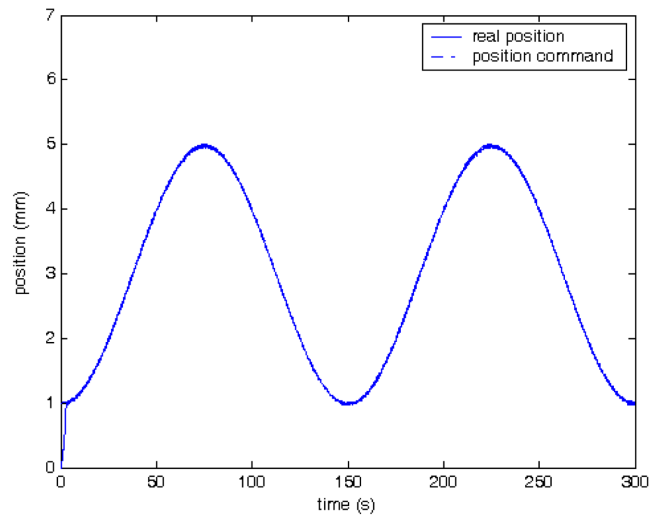


Fig. 10 The actual trajectory following a 1/150 Hz sinusoidal command

position. The response in this case is shown in Fig. 9. Obviously in the two figures, the position responses are much faster than those of open-loop testing and the steady state errors are very small. The transient performance is satisfactory as there is no overshoot. Stability of the system is ensured during the entire regulation tasks.

For the position tracking, the task is to follow a 1/150 Hz sinusoidal wave. The maximum and minimum values of the wave are 5 mm and 1 mm respectively. Fig. 10 shows the actual trajectory and the desired trajectory. It is evident that the actual movement of the intake system closely follows the desired trajectory. The tracking error is shown in Fig. 11. The root-mean-square error is 0.03 mm.

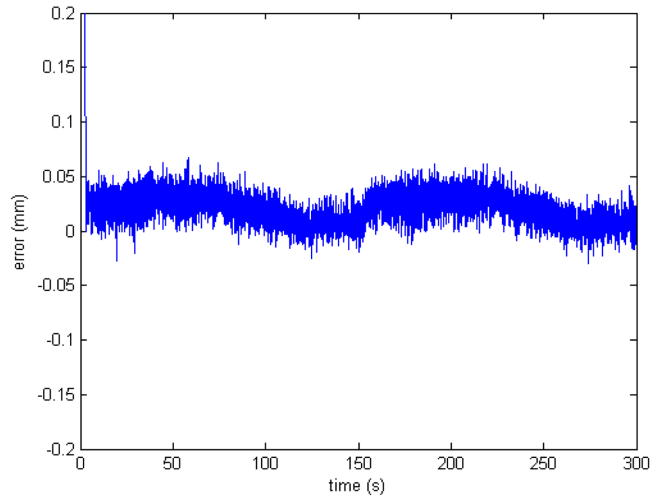


Fig. 11 The tracking error

## 6. Conclusions

In this paper, a novel design of SMA wire actuated variable area engine intake along with its testing and feedback control are presented. Open-loop testing of the intake model is conducted to verify the functionality of the proposed intake model. It was observed that 25% area reduction of the intake model can be achieved. Based on the open-loop testing results, a sliding mode based robust controller was designed and implemented. Experiments of both position regulation and trajectory tracking are carried out and the results demonstrate that the model engine intake achieves desired performance with the proposed robust controller. Future research will involve 1) Thermal analysis of the SMA actuator at a cold environment to calculate the require power consumption for actuation, 2) The dependence of the operating bandwidth of the SMA actuator on the environmental temperature, 3) Design of appropriate insulation for the SMA actuator to achieve an optimal compromise between the operating bandwidth and the required energy for actuation at a cold environment and 4) Tests of the intake model with SMA actuation at a cold environment.

## Acknowledgements

The first author would like to thank for the supports provided by NASA via a cooperative grant (No. NCC3-939-1) and NSF via a CAREER grant (Grant No. 0093737). Any opinions, findings and conclusions or recommendations expressed in this material are those of the author(s) and do not necessarily reflect the views of the sponsors. This research is also partially supported an internal grant from the Institute of Space Systems Operations (ISSO) at the University of Houston.

## References

Baroah, P. and Rey, N. (2002), "Closed loop control of a shape memory alloy actuation system for variable area

- fan nozzle”, *Proceedings of the SPIE International Symposium on Smart Structures and Materials*, **4693**, 384-395.
- Barbarino, S., Pecora, R., Lecce, L., Concilio, A., Ameduri, S. and Calvi, E. (2009), “A novel SMA-based concept for airfoil structural morphing”, *J. Mater. Eng. Perform.*, **18**(5-6), 696-705.
- Calkins, F.T., Mabe, J.H. and Butler, G.W. (2006), “Boeing’s variable geometry chevron: Morphing aerospace structures for jet noise reduction”, *Proceedings of the SPIE - The International Society for Optical Engineering*, **6171**.
- Choi, S.B., Han, Y.M. and Cheong, C.C. (2001), “Force tracking control of a flexible gripper featuring shape memory alloy actuators”, *Mechatronics*, **11**(6), 677-690.
- Dayananda, G.N., Varughese, B. and Subba Rao, M. (2007), “Shape memory alloy based smart landing gear for an airship”, *J. Aircraft*, **44**(5), 1469-1477.
- Epps, J. and Chopra, I. (2001), “In-flight tracking of helicopter rotor blades using shape memory alloy actuators”, *Smart Mater. Struct.*, **10**(2001), 104-111.
- Grant, D. and Hayward, V. (1997), “Variable structure control of shape memory alloy actuator”, *IEEE Contr. Syst. Mag.*, **17**(3), 80-88.
- Majima, S., Kodama, K. and Hasegawa, T. (2001), “Modeling of shape memory alloy actuator and tracking control system with the model”, *IEEE T. Contr. Syst. T.*, **9**(1), 54-59.
- Peng, F., Jiang, X., Hu, Y. and Ng, A. (2009), “Application of SMA in membrane structure shape control”, *IEEE T. Aero. Elec. Sys.*, **45**(1), 85-93.
- Pitt, D.M., Dune, J.P., White, E.V. and Garcia, E. (2001), “Wind tunnel demonstration of the SMAPON smart inlet”, *Proceedings of the SPIE International Symposium on Smart Structures and Materials*, **4332**, 345-356.
- Rey, N.M., Tillman, G., Miller, R.M., Wynosky, T., Larkin, M.J., Flamm, J.D. and Bangert, L.S. (2001), “Shape memory alloy actuation for a variable area fan nozzle”, *Proceedings of the SPIE International Symposium on Smart Structures and Materials*, **4332**, 371-382.
- Song, G. and Mukherjee, R. (1998), “A comparative study of conventional non-smooth time-invariant and smooth time-varying robust compensators”, *IEEE T. Contr. Syst. T.*, **6**(4), 571-576.
- Song, G. and Quinn, D. (2000), “Robust tracking control a shape memory alloy wire actuator”, *Proceedings of the Symposium on Control of Vibration and Noise at ASME International Mechanical Engineering Congress and Exposition*.
- Strelec, J.K., Lagoudas, D.C., Khan, M.A. and Yen, J. (2003), “Design and implementation of a shape memory alloy actuated reconfigurable airfoil”, *J. Intel. Mater. Syst. Str.*, **14**(4-5), 257-273.
- Wolf, W. and Gunter, P. (2001), “Shape adaptive structures for smart airfoils”, *Proceedings of the IEEE International Conference on Multisensor Fusion and Integration for Intelligent Systems*, Baden-Baden, Germany, August.

## Appendix

### 1. Derivation of Eqs. (1) and (2)

Assume the SMA wire has a  $\Delta x$  change in the length. Then, it can be derived that  $\Delta x = 2\pi\Delta R$ . As shown in Fig. 4,  $R=AH$ ,  $R=CG$ ,  $\Delta R=AH-CG$ . In order to obtain  $CG$ , we will first calculate  $CD$  and  $DG$ , respectively.

$$CD = CE \cos\Delta\theta = AB \cos \Delta\theta$$

$$DG = EF = BH - OE \sin \Delta\theta = R - AB - OB \sin \Delta\theta$$

then  $CG = CD + DG = AB \cos \Delta\theta + R - AB - OB \sin \Delta\theta$

$$\Delta R = AH - CG = R - (AB \cos \Delta\theta + R - AB - OB \sin \Delta\theta) = AB + OB \sin \Delta\theta - AB \cos \Delta\theta \quad (7)$$

On the other hand, the intake area is  $A = \pi r^2$ , therefore  $\Delta A = 2\pi r \Delta r$ .

Now, it can be found that  $\Delta r = L \sin \Delta\theta$  from the geometry, as shown in Fig. 4. Then  $\Delta A = 2\pi r L \sin \Delta\theta$  or

$$\sin \Delta\theta = \frac{\Delta A}{2\pi r L} \quad (8)$$

Substituting Eq. (8) into Eq. (7) gives

$$\Delta R = AB + OB \sin \Delta\theta - AB \cos \Delta\theta = AB + OB \frac{\Delta A}{2\pi r L} - AB \sqrt{1 - \left(\frac{\Delta A}{2\pi r L}\right)^2}$$

therefore,

$$\Delta x = 2\pi\Delta R = 2\pi \left[ AB + OB \frac{\Delta A}{2\pi r L} - AB \sqrt{1 - \left(\frac{\Delta A}{2\pi r L}\right)^2} \right]$$

or

$$\Delta x = 2\pi\Delta R = 2\pi \left[ AB + OB \frac{\Delta r}{L} - AB \sqrt{1 - \left(\frac{\Delta r}{L}\right)^2} \right]$$

### 2. Derivation of Eqs. (3) and (4)

The maximum value of  $\Delta\theta$  is around 5 degrees, therefore we can use the following approximations:  $\sin \Delta\theta = \Delta\theta$ ,  $\cos \Delta\theta = 1$ . Subsequently Eq. (7) can be written as

$$\Delta R = AB + OB \sin \Delta\theta - AB \cos \Delta\theta = OB \Delta\theta \quad (9)$$

and Eq. (8) can be simplified to

$$\sin \Delta\theta = \Delta\theta = \frac{\Delta A}{2\pi r L}. \quad (10)$$

Substitute Eq. (10) into Eq. (9), we get

$$\Delta R = OB\Delta\theta = OB\frac{\Delta A}{2\pi rL} = \frac{OB}{2\pi rL}\Delta A$$

therefore

$$\Delta x = 2\pi\Delta R = 2\pi\frac{OB}{2\pi rL}\Delta A = \frac{OB}{rL}\Delta A$$

or

$$\Delta x = \frac{OB}{rL}\Delta A = \frac{OB}{rL}2\pi r\Delta r = \frac{2\pi OB}{L}\Delta r$$